The properties of ion-water clusters. I. The protonated 21-water cluster

Srinivasan S. Iyengar[a)]
Department of Chemistry and Department of Physics, Indiana University, 800 East Kirkwood Avenue, Bloomington, Indiana 47405

Matt K. Petersen, Tyler J. F. Day, and Christian J. Burnham
Department of Chemistry and Center for Biophysical Modeling and Simulation, 315 South 1400 East Room 2020, University of Utah, Salt Lake City, Utah 84112-0850

Virginia E. Teige
Department of Chemistry and Department of Physics, Indiana University, 800 East Kirkwood Avenue, Bloomington, Indiana 47405

Gregory A. Voth[b)]
Department of Chemistry and Center for Biophysical Modeling and Simulation, 315 South 1400 East Room 2020, University of Utah, Salt Lake City, Utah 84112-0850

(Received 25 April 2005; accepted 1 July 2005; published online 29 August 2005)

The *ab initio* atom-centered density-matrix propagation approach and the multistate empirical valence bond method have been employed to study the structure, dynamics, and rovibrational spectrum of a hydrated proton in the "magic" 21 water cluster. In addition to the conclusion that the hydrated proton tends to reside on the surface of the cluster, with the lone pair on the protonated oxygen pointing "outwards," it is also found that dynamical effects play an important role in determining the vibrational properties of such clusters. This result is used to analyze and complement recent experimental and theoretical studies. © *2005 American Institute of Physics*. [DOI: 10.1063/1.2007628]

I. INTRODUCTION

The stability, orientation, and structural features of protonated and unprotonated water clusters[1–10] have significance for biological,[11–14] atmospheric,[15,16] and condensed phase chemistry. Protonated water clusters have been the subject of a rich experimental[2,17–25] and theoretical literature.[1,26–49] Early mass-spectrometric studies[21,22,50] on protonated clusters revealed $H^+(H_2O)_{21}$ and $H^+(H_2O)_{31}$ to have greater stability as compared to clusters of similar sizes. Due to this fact, the well-studied $H^+(H_2O)_{21}$ species has often been referred to as a "magic number" cluster and its additional stability has been proposed as the reason for its greater abundance in the earth's stratosphere.[21,50]

Recently, Shin *et al.*[1] and Miyazaki *et al.*[2] have reported detailed infrared data and theoretical studies for small clusters including $H^+(H_2O)_{21}$. The authors have independently shown that the spectral features observed for the dangling hydroxyl bond stretch collapse into a single feature for 21- and 22-molecule clusters then reemerge as a multiplet for 23-molecule and larger clusters. This result is complemented by a recent study conducted by Wu *et al.*[4] The authors[4] performed mass-spectrometric and infrared studies in conjunction with Monte Carlo sampling of the 21-mer potential energy and *ab initio* single-point optimization and frequency calculations. They note that at low-pressure conditions, the dangling OH stretch has the propensity to display a weak doublet which is due to open noncagelike configurations that may be visited as part of the experimental ensemble sampling. These simulations imply that all dangling bonds in the 21- and 22-molecule clusters arise from molecules at remarkably similar binding sites. Miyazaki *et al.*,[2] through spectral changes with increasing cluster size, have also concluded the existence of three distinct morphological forms in protonated water clusters. Protonated clusters with less than ten water molecules form chain structures. For clusters containing 10–21 water molecules the hydrogen-bond network conforms to a two-dimensional sheet or net structure. The hydronium in both the network and chain topologies donates all three hydrogens to bonds with neighboring molecules and is hence at the center of the bonding network although there is no clear interior for clusters of such size. The authors noted that conversion from the network structure to nanometer-scaled cages occurs in clusters with 21 water molecules or more. Shin *et al.*[1] carried out a number of electronic structure studies on low-energy isomers of 21- and 22-molecule clusters and concluded that the arrangements with an interior hydronium were on average $\approx$9 kcal/mol higher in energy than those with the hydronium on the cluster surface. However, the experimental and theoretical IR spectral studies were not in agreement[1] concerning the modes accessible for hydroxyl stretch in the protonated species.

In the current paper we examine the behavior of the "magic number" 21-water protonated cluster at a variety of different temperatures using an *ab initio* molecular-dynamics approach called atom-centered density-matrix propagation[51–56] (ADMP) and the second-generation multi-

[a)]Electronic mail: iyengar@indiana.edu
[b)]Electronic mail: voth@chem.utah.edu

 © 2005 American Institute of Physics

Downloaded 01 Sep 2005 to 129.79.138.80. Redistribution subject to AIP license or copyright, see http://jcp.aip.org/jcp/copyright.jsp

state empirical valence bond[57] (MS-EVB2) model. The latter model, combined with the parallel basin hopping and tempering (PBHaT) algorithm, which will be reported in a forthcoming paper,[58] enabled an efficient and complete sampling of the potential surface at many different temperatures. In addition we employ single-point optimization and frequency calculations on snapshots obtained from the ADMP simulations, and MP2 calculations using large basis sets to examine and confirm our results. The experimental frequency calculations are compared with the vibrational spectrum obtained directly from ADMP simulation data at finite temperature, which thereby includes dynamical effects. This leads to interesting interpretations of the spectroscopic work of Shin *et al.*[1] Radial distribution functions obtained from ADMP further quantify these results and show that both Zundel and Eigen cation forms of the hydrated proton are present in our dynamics simulation. In addition, our ADMP simulations demonstrate that the conformations having the protonated species on the surface could be anywhere between 10 and 20 kcal/mol more stable compared to structures with the protonated species in the interior. We also present initial studies on the spectroscopic change due to the presence of argon interacting with this cluster, since argon is used as a messenger in previous experimental spectroscopic studies.[19,59]

The paper is organized as follows: In Sec. II the computational methods used in this study are briefly outlined. In Sec. III the dynamics results are described where it is seen that the protonated species spontaneously migrates to the surface of the cluster. In Sec. III the vibrational properties of this cluster, obtained from the dynamics, are also analyzed in detail while in Sec. IV conclusions are presented.

II. COMPUTATIONAL METHODOLOGY

The simulations in this paper were carried out using an *ab initio* molecular-dynamics approach called ADMP,[51–56] the second generation MS-EVB2 (Ref. 57) approach, and PBHaT.[58] The ADMP simulations were carried out using the Gaussian series of electronic structure programs.[60] The MS-EVB2 simulations were conducted using a modified version of the DL_POLY (Ref. 61) simulation package. The results were further confirmed through post-Hartree-Fock MP2 calculations using a large triple-zeta polarized-diffused basis set. ADMP has been shown to be accurate and efficient in studying the dynamics of medium- to large-sized systems in the multipicosecond time scale.[51–56] MS-EVB has been successfully used to treat proton transport in water[57,62–65] and a variety of aqueous and biomolecular systems.[66–72] MS-EVB is a partially polarizable model where the charge distribution is dynamic and it reproduces the Zundel versus Eigen behavior very well.

In ADMP the choice of basis set and density functional is critical. To help in making the proper choice, a detailed analysis was conducted using a variety of basis functions and density functionals (such as B3LYP, BLYP, and BPBE) for the water dimer system, with and without basis-set superposition error.[56] Based on these results, the B3LYP and BPBE density functionals with the double-zeta polarized-diffused 6-31+G** basis were chosen for all ADMP simulations. Higher-level MP2 calculations using a triple-zeta polarized-diffused basis, 6-311++G**, were used to further validate our ADMP results. A time step of 0.25 fs in ADMP and a valence fictitious mass of 180 a.u., along with a tensorial mass-weighting scheme, were employed as in earlier studies.[52] Two different kinds of ADMP simulations were performed to study the system. The first set of simulations were performed under constant temperature (*NVT*) conditions and results from these simulations were used to analyze structural features of the water cluster. The constant temperature condition was enforced through velocity scaling. The instantaneous temperature in this case was calculated assuming equipartition theorem, and it was found that approximately 95% of the configurations were within 10 K from the target temperature, which was considered satisfactory. A second simulation was then performed at constant energy (*NVE*) starting from a final *NVT* simulation configuration. The results from this simulation were used to analyze the dynamical properties calculated using time correlation functions.

The MS-EVB2 simulations using the PBHaT algorithm were carried out as described in a forthcoming paper.[58]

III. RESULTS AND DISCUSSION

The NVT ADMP simulations were performed at 150, 200, and 300 K using B3LYP/6-31+G** and BPBE/6-31+G** levels of density-functional theory (DFT) and Gaussian basis set. Three different starting geometries were considered for enhanced sampling. (The simulations are summarized in Table I for clarity.) All of the starting geometries had the proton fully solvated in the center of the cluster. The starting geometry for the first set of simulations was a regular dodecahedron, with the hydronium in the center. This structure was originally proposed by Yang *et al.*[21] The associated set of ADMP simulations conducted at 150, 200, and 300 K using B3LYP/6-31+G** and BPBE/6-31+G** (that is six different ADMP simulations) are together represented as simulation I in the discussion below. The second starting geometry was obtained from a gradient optimization of the starting geometry used in simulation I. The geometry optimization was performed using a polarizable water model[73] and the corresponding ADMP dynamics, conducted at 200 K using B3LYP/6-31+G**, is represented as simulation II. (The starting geometry for simulation II leads to the lowest-energy conformation that we found, which still had the protonated species on the interior of the cluster.) A third starting geometry was obtained from equilibration of the second structure using MS-EVB2. The associated ADMP trajectory, also conducted at 200 K using B3LYP/6-31+G**, is represented as simulation III. All of these simulations are used to study the structural features of the cluster and our results are described in Sec. III A. In addition, for further sampling of the cluster potential surface and to understand the behavior of the system at multiple temperatures, we have also conducted PBHaT studies with the MS-EVB2 model at temperatures ranging from 100 to 450 K. PBHaT (Ref. 58) is a parallel tempering[74] scheme that allows switching between multiple-temperature simulations based on a basin hopping[75]

Downloaded 01 Sep 2005 to 129.79.138.80. Redistribution subject to AIP license or copyright, see http://jcp.aip.org/jcp/copyright.jsp

TABLE I. Summary of ADMP simulations performed under *NVT* conditions for structural analysis. The simulations are described in Sec. III A.

	Simulation I[a]						Simulation II[b]	Simulation III[c]
Temperature (K)	150		200		300		200	200
DFT functional[d]	B3LYP	BPBE	B3LYP	BPBE	B3LYP	BPBE	B3LYP	B3LYP

[a]Represents the simulations performed using a regular dodecahedron starting geometry, with the hydronium in the center. This structure was originally proposed by Yang *et al.* (Ref. 21).
[b]Represents the simulations performed using a starting geometry obtained from gradient optimization of the starting geometry used in simulation I. The geometry optimization was performed using a polarizable water model (Ref. 73).
[c]Represents the simulations performed using a starting geometry obtained from equilibration of the starting geometry used in simulation II. The equilibration was performed using MS-EVB2.
[d]All calculations used the 6-31+G** Gaussian basis set.

modification of Metropolis sampling. It thus combines the benefits of the basin hopping approach with parallel tempering to achieve enhanced sampling of the potential-energy surface. This algorithm is more completely described in a forthcoming paper.[58]

To perform infrared spectroscopic studies, independent ADMP *NVE* simulations were conducted which are described in Sec. III B.

A. Structural properties: Amphiphilicity of the hydrated proton

The evolution of the protonated species was followed in real time. In both ADMP and MS-EVB2 the definition of the protonated species can change during the dynamics process, since the proton hops along an optimal conformation of water molecules consistent with the Grotthuss mechanism of proton transfer.[5–10] The migration or shuttling of the excess proton was monitored and the number of water molecules on the surface side of the protonated species tracked. A ball-rolling algorithm based on the Connolly solvent accessible surface area[76] was also used to monitor the progress of the protonated species. In all the simulations the number of water molecules on the surface side of the protonated species reduced and the excess proton gradually migrated to the surface of the cluster. This observation is consistent with our earlier studies where a similar effect was seen for protonated water clusters[77] and acidified water/vacuum interfaces.[65] After reaching the surface, the protonated species continued to hop across the hydrogen-bond network existing among the surface water molecules. The lone pair on the most protonated oxygen atom was directed outwards from the cluster as seen in our earlier studies[65,77] which reinforces the concept that the protonated species in water clusters has "hydrophobic" and "hydrophilic" sites, the hydrophobic region being in the vicinity of the lone pair on the oxygen atom.[65,77] In Fig. 1 we present the evolution of the hydrated proton during simulation II. The cluster size is also indicated to show the surface proximity of the hydrated proton. The cluster size is computed using the distance of the farthest oxygen from the cluster center.

ADMP simulations I and III proceeded downhill on the potential surface towards more stable structures with the proton on the exterior region. For simulation II the proton is ejected to the surface within 1 ps. The protonated species remained on the surface for the rest of the simulation (5.5 ps). However, the conformations obtained during this dynamics with the proton on the surface had potential energy higher than the starting structure. To compare the topography of the potential-energy surface in the region where the proton is in the interior with the topography of the surface when the proton is on the surface, snapshots were obtained from simulation II. The B3LYP level of density-functional theory with a double-zeta polarized-diffused basis set, 6-31+G**, was employed to optimize these snapshot configurations. These optimized snapshots provided a family of "inherent" structures to represent the dynamical trajectory and revealed that the configurations with the proton on the exterior may be about 10–20 kcal/mol lower in potential energy as compared to the local minima with the proton on the interior (see Fig. 2). Higher-level MP2 calculations using larger triple-zeta polarized-diffuse basis functions, 6-311++G**, were used to further confirm these results. Additional analysis of the components of the total electronic energy in the ADMP simulations lead to the interesting observation that the nuclear-nuclear repulsion energy and electron-electron correlation energy are in fact larger for the configurations that have the proton on the surface. This is, however, more than

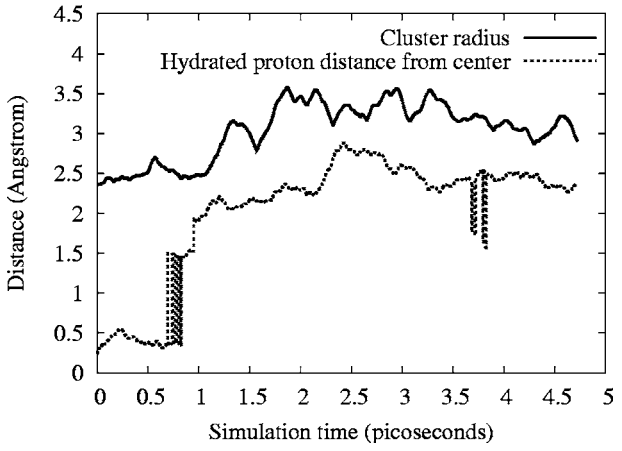

FIG. 1. Time evolution of the protonated species for the $H^+(H_2O)_{21}$ cluster obtained from simulation II (B3LYP/6-31+G**). The hydrated species clearly accomplishes a sequence of hops that takes it closer to the surface of the cluster as noted for larger systems in Refs. 65 and 77.

Downloaded 01 Sep 2005 to 129.79.138.80. Redistribution subject to AIP license or copyright, see http://jcp.aip.org/jcp/copyright.jsp

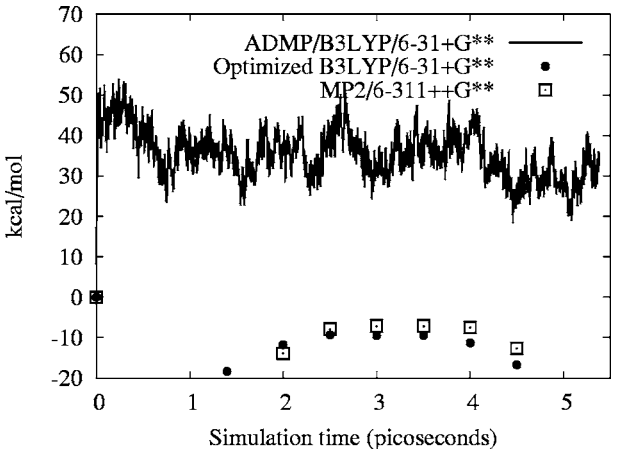

FIG. 2. The progression of the electronic energy during ADMP simulation II at 200 K. All conformations beyond ≈0.5 ps have the proton on the surface of the cluster. The solid circles represent optimized energies of structures obtained from the ADMP simulation. The surface geometries are noted to have lower energies compared to the interior structures and this is further substantiated by the energies of optimized geometries recalculated using the MP2 level of theory (open squares in the figure) and a larger basis set (6 -311++G**). All energies are relative to the optimized geometry at initial time.

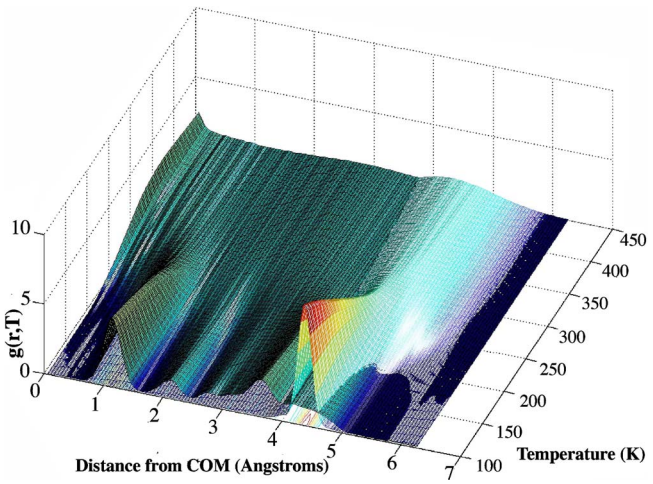

FIG. 3. (Color online) Radial distribution function for water and the proton center of excess charge (CEC) as a function of temperature, obtained using the parallel basin hopping and tempering (PBHaT) algorithm. The figure reflects both the melting of the cluster (water is dark shade) in the range of 150–200 K and the fact that the excess proton (light shades) is always on the surface over the whole temperature range, in agreement with the ADMP results.

compensated for by a large reduction in the electron-nuclear attraction energy. It was further noted that the electronic kinetic energy was marginally lower when the protonated species was on the surface, thus adding to its energetic stabilization.

The effects due to nuclear-nuclear repulsion energy and electron-electron correlation energy are quite interesting and seems to further rationalize our earlier conclusions that the hydrated proton is in some ways amphiphillic. The increase in nuclear-nuclear repulsion energy as the proton goes to the surface indicates that the average distance between most nuclei in the "surface" configuration is less than the average distance between these for the configurations with the proton in the interior of the cluster. This indicates that the proton is "squeezed" out of the nanodroplet and this is very much reminiscent of the effect seen from the ejection of a hydrophobe from the interior of a water cluster. A similar analysis of the fact that the electron-electron correlation energy increases as the proton becomes surface bound leads to the same conclusion.

This intriguing "ejection" of the protonated species to the surface found in our simulations is consistent with our earlier predictions on the protonated water cluster system[77] and water/vacuum interfaces.[65] A similar structure has been used in Ref. 1 to compare experimental and theoretical infrared spectra. (This aspect is discussed in further detail in Sec. III B.) However, these results are different from earlier studies by Castleman and co-workers,[21,50] who proposed a structure for this system with the hydronium at the center of a clathrate formed by 20 water molecules. The structure proposed in Refs. 21 and 50 was the starting geometry of our simulation I which resulted in the spontaneous removal of the hydrated proton from the interior of the cluster. The experimental prediction in Refs. 21 and 50 was based on a clever titration experiment where the cluster was titrated with trimethylamine (TMA) that binds to nonbonded hydrogen atoms. It was found[21] that up to ten TMA molecules bind to the $H^+(H_2O)_{21}$ cluster, leading these authors to conclude that there must be up to ten hydrogen atoms "dangling" outwards from the cluster with no hydrogen bonds. To explain this observation, they proposed a clathratelike structure formed by 20 water molecules,[21] with ten dangling hydrogen atoms, and with the excess hydronium located at the center of the 20-water clathrate. For all of our ADMP trajectories, however, the change in the number of non-hydrogen-bonded dangling hydrogen atoms was monitored during the simulation, and it was found that this number remained close to ten (fluctuating between 9 and 11) throughout the simulation, thus being consistent with the experimental result. However, by contrast most of the structures obtained in the present simulations have the protonated species on the surface.

To further understand this amphiphilic behavior of the protonated species we have conducted PBHaT studies on the 21-mer and the results are depicted in Fig. 3. Shown here is a plot of the water probability density (dark shade) and the probability density of the excess protonic charge center (light shade) as a function of the distance from the cluster center along one axis and the temperature along the other axis. For a fixed temperature a slice along the distance axis is essentially the radial distribution function for the water or excess proton (depending on the shade in the figure) from the center of the cluster. At low temperatures the excess proton density is strongly peaked and on the surface of the cluster. As the temperature is increased, the distribution of excess proton density begins to broaden while maintaining a strong presence on the surface. At the same time, as the temperature is increased the water cluster begins to melt (in the temperature range of 150–200 K) and some open noncagelike structures begin to become important at the highest temperatures. Hodges and Wales[75] and Wu *et al.*[4] have performed Monte Carlo searches for the global minimum of protonated water clusters using different potential-energy functions and also

Downloaded 01 Sep 2005 to 129.79.138.80. Redistribution subject to AIP license or copyright, see http://jcp.aip.org/jcp/copyright.jsp

predict the global minimum (0 K) to have the proton on the exterior of the cluster. This is consistent with the present detailed computational results as a function of temperature.

B. Analysis of vibrational spectrum: Comparison to experiment

The vibrational properties of the cluster were analyzed in several ways. Harmonic frequency calculations were performed on the inherent structures of ADMP dynamics obtained from the geometry optimization described above (and in Fig. 2). Rovibrational density of states were obtained from the Fourier transform of the velocity-velocity autocorrelation function and a vibrational spectrum inclusive of all dynamical effects was obtained by calculating the Fourier transform of the dipole-dipole autocorrelation function. Quantum-nuclear corrections were included in the dipole-dipole autocorrelation function, within the harmonic approximation.[78,79] Separate constant *NVE* ADMP simulations were performed for calculating the time correlation functions, and these were started from the final structure obtained from the 5.5-ps *NVT* simulation II described in Sec. III A. The *NVE* simulation had an average temperature of 250 K, which should be above the cluster melting point, with a deviation of ±20 K. Temperature control was not exercised during these simulations since, in this section, we were interested in computing dynamical information through time correlation functions. The length of the *NVE* simulation was 8.5 ps. The results are shown in Figs. 4 and 5. Figures 4(a)–4(c) show the harmonic frequencies for the inherent structures at 0, 1.4, and 2.5 ps. As can be seen the peaks in the 2000–3000-cm^{-1} frequency region change in character substantially during the simulation. This is the O–H stretch region for the protonated species and since the environment of the protonated species changes substantially during the simulation, by way of proton hopping which affects various bonding topology changes, the corresponding vibrational spectrum also changes its features. We further note that the inherent structures thus obtained comprise neither pure Zundel nor pure Eigen states and are in fact mixed states. This aspect of mixed Zundel-Eigen states is also seen in Fig. 6 where the radial distribution function of the distance between the most protonated oxygen and the rest of the unprotonated oxygen atoms is presented. The inset shows a broad feature between ~2.44 and ~2.65 Å. Based on our calculations at the B3LYP/6-31+G^{**} level and on previous studies,[31] we note that pure Zundel structures have an oxygen-oxygen distance of about 2.45 Å and pure Eigen structures have this distance at 2.55 Å. Thus the broad feature indicates the presence of both these species in the simulations, as is obvious from the fact that proton hopping primarily occurs through an Eigen →Zundel→Eigen transition. This character is also seen in the inherent structures. An example Zundel structure found during the ADMP simulations is shown in Fig. 7.

The rovibration density of states and IR spectrum obtained from ADMP are shown in Figs. 5(a) and 5(b). The vibrational density of states intensity is obtained from the Fourier transform (FT) of the nuclear velocity-velocity autocorrelation (VAC) function from the ADMP dynamics. The

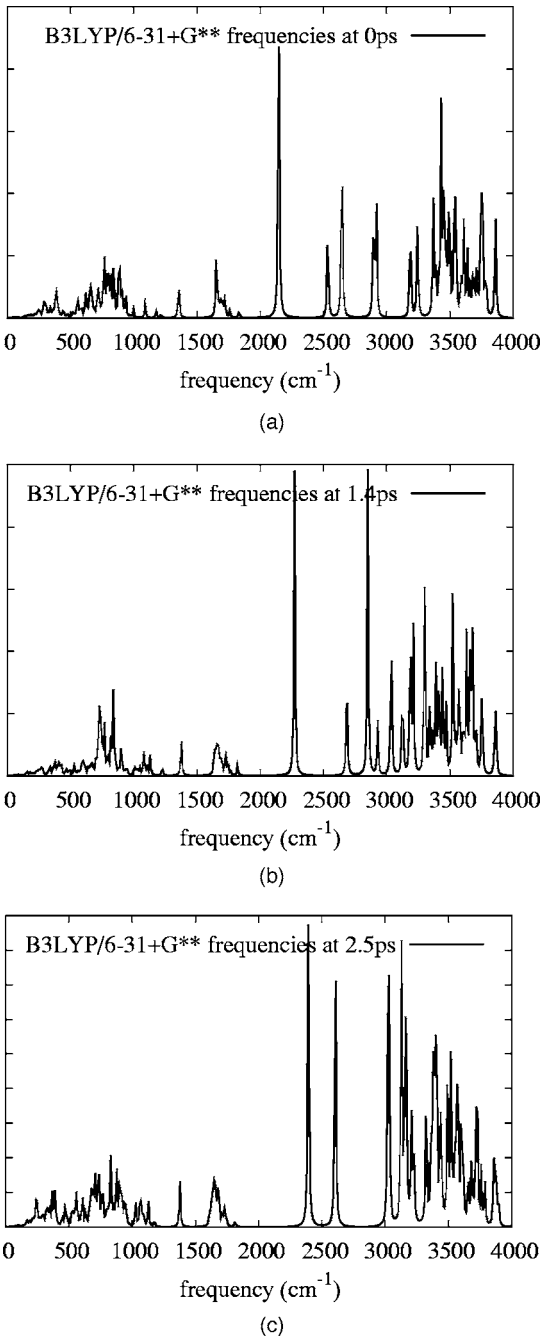

FIG. 4. Panels (a)–(c) show the harmonic frequencies obtained from the optimized geometries at 0, 1.4, and 2.5 ps of ADMP simulation II, respectively (see Fig. 2.) Note the frequency shift in the 2000–3000-cm^{-1} range in panels (a)–(c). This corresponds to the O–H stretch of the protonated species. See discussion and Fig. 5 for details.

IR spectrum inclusive of dynamical effects is obtained from the Fourier transform of the dipole-dipole autocorrelation (DAC) function. Consequently, the FT-DAC (Ref. 80) is expected to be close to the IR spectrum, while the FT-VAC may be expected to be similar to a deep inelastic neutron-scattering experimental measurement. We use both spectra to analyze our results. The FT-VAC is useful since the existence of intensity at a certain frequency indicates the existence of a vibrational state. This state, however, may include motion that does not exhibit a change in dipole and hence may not be IR active. In this case it would not be seen in the FT-

Downloaded 01 Sep 2005 to 129.79.138.80. Redistribution subject to AIP license or copyright, see http://jcp.aip.org/jcp/copyright.jsp

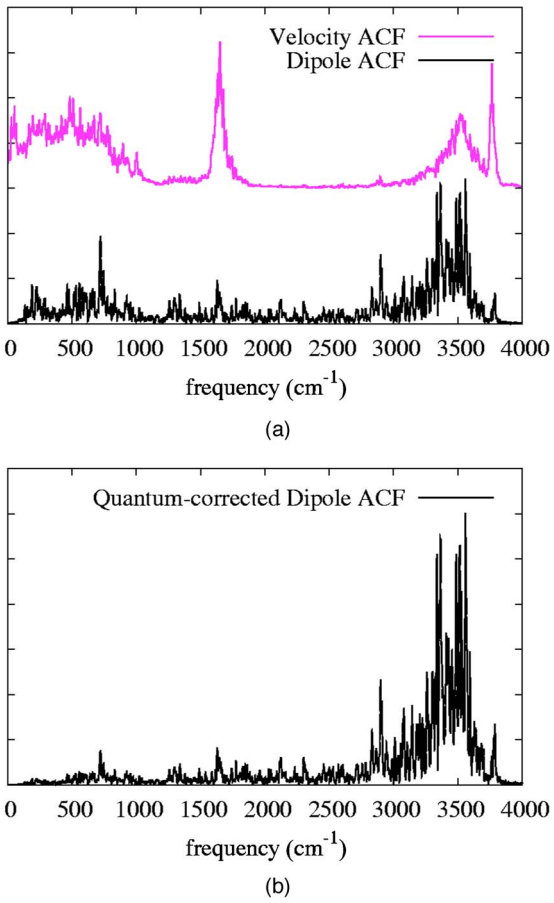

FIG. 5. (Color online) Panel (a) shows the Fourier transform of the velocity-velocity autocorrelation function (also known as the vibrational density of states) obtained from the ADMP simulations (top spectrum) and the Fourier transform of the dipole-dipole autocorrelation function (bottom spectrum). Note that the intensities in the 2000–3000-cm^{-1} range in Figs. 4(a)–4(c) are minimal for the velocity-velocity autocorrelation function and greatly broadened for the dipole-dipole autocorrelation function. See discussion for details. The dipole correlation function including quantum-nuclear corrections shown in (b) further accentuates this effect. The peak from the dangling O–H bonds at the highest frequency is evident in all the figures.

DAC. On the other hand, a state may exhibit a large change in dipole leading to a larger intensity in the FT-DAC. This distinction is important in the following discussion.

The FT-VAC and FT-DAC results are first summarized before analyzing the details. It should be noted that the FT-VAC in Fig. 5 is quite similar to the experimental spectrum in Ref. 1, but the FT-DAC deviates in having a lower intensity of the free O–H stretch peak. This is similar to the difference seen between theory and experiment in Ref. 1. It is further important to note that the spectrum in Ref. 2 does provide a peak lower in intensity consistent with our results and the theoretical results in Ref. 1. Most importantly, the features in the 2000–3000-cm^{-1} frequency range seen in Figs. 4(a)–4(c) are largely absent in Fig. 5(a) except for a small peak at 2900 cm^{-1} in the FT-VAC, which is accentuated in the FT-DAC. This overall reduction in intensity in the 2000–3000-cm^{-1} frequency range is further emphasized when quantum-nuclear corrections are included in Fig. 5(b) where the FT-DAC in Fig. 5(a) is multiplied by the correction factor[81] $\beta\hbar\omega/[1-\exp(-\beta\hbar\omega)]$ where $\beta=1/k_BT$, and $\omega=2\pi/\lambda$, to obtain the quantum dipole autocorrelation with

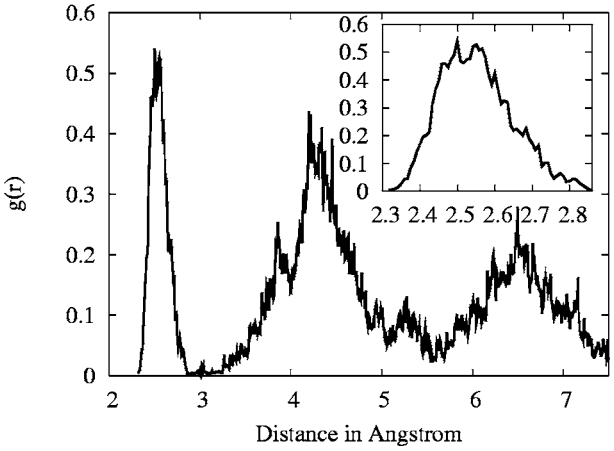

FIG. 6. The radial distribution function for the distance between the protonated water and all other water molecules in the cluster. The inset shows the signature of both Zundel (2.45 Å) and Eigen (2.55 Å) species. Such a Zundel ion found during ADMP simulation I is shown in Fig. 7.

"harmonic corrections." This expression is exact in the limit where the dipole operator is a linear combination of degrees of freedom that are well described by a harmonic Hamiltonian.[78,79]

This lowering of intensity in the 2000–3000-cm^{-1} frequency range is intriguing since the three panels of Fig. 4 were obtained from geometry optimization of configurations sampled during ADMP simulations. While the rest of the features are retained in Fig. 5, the intensities in the 2000–3000-cm^{-1} range seem to be "washed out" in the velocity-velocity autocorrelation function and "broadened" in the dipole-dipole autocorrelation function. [The dipole-dipole autocorrelation function typically requires a longer simulation time to converge as compared to the velocity-velocity autocorrelation which is indicated by its more noisy

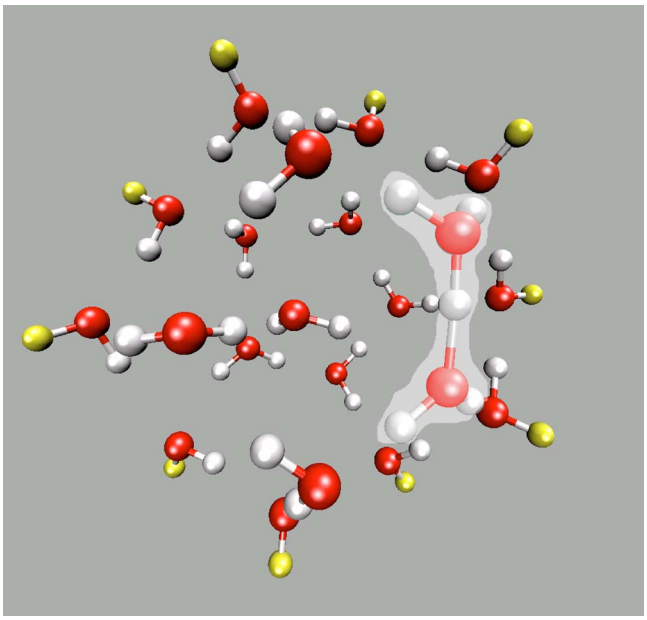

FIG. 7. (Color online) A geometry obtained during ADMP B3LYP/6-31+G** simulation I. The protonated species on the surface (a Zundel in this case) is highlighted and the ten "dangling" hydrogens are also seen. All other hydrogens are shown using light spheres.

Downloaded 01 Sep 2005 to 129.79.138.80. Redistribution subject to AIP license or copyright, see http://jcp.aip.org/jcp/copyright.jsp

appearance in Fig. 5(a)]. This underlines the fact that the minimum-energy conformations used in the three panels of Fig. 4, although sampled during an ADMP ensemble averaging, do not have high enough statistical weights. Many other configurations (thermal fluctuations) also play an important role in the statistical sampling.

The experimental vibrational spectrum in Ref. 1 is very similar to the FT-VAC we find in Fig. 5(a); the FT-DAC on the contrary shows more noise and longer simulations are necessary to correct this. The FT-DAC with quantum corrections in Fig. 5(b) is also in closer agreement with the experiments in Refs. 1 and 2. In Figs. 5(a) and 5(b) the features in the 2000–3000-cm^{-1} frequency range are reduced in intensity or absent as in the experiment.[1] The 0-K theoretical results in Ref. 1 are, however, similar to what we obtain in Figs. 4(a)–4(c). The *dynamical* behavior of the cluster may have an important role in the experimental observation. This leads us to the conclusion that the experiment (like the ADMP dynamics simulation) at a finite temperature does not sample the optimized 0-K structures with high probability. Furthermore, the autocorrelation functions are a dynamical property that can be thought of as being obtained as a statistical average of many different configurations, only three of which are contained in the panels shown in Fig. 4. Due to the change in the vibrational intensities in the 2000–3000-cm^{-1} region during dynamics (from anisotropic and anharmonic changes in environment of the protonated species), the statistical average broadens and flattens this region out. Furthermore, Fig. 5(b) indicates that quantum-nuclear effects might play an additional role in this reduction of relative intensity. This aspect along with an understanding of the regions of the potential-energy surface dynamically sampled during the experiment (and dynamics simulation) is critical to fathom the differences seen in Ref. 1. Of course, conformational sensitivity of IR spectra is not a new concept[82] and has been known in conformational analysis[83] for a long time.

C. Effect of argon

While the FT-VAC shown in Fig. 5 is similar to that seen in the experimental results of Ref. 1, the FT-DAC differs by having a much lower intensity for the free OH stretch. This is also the case for the three panels in Fig. 4 and also the case for the theoretical result in Ref. 1. Furthermore, at 2900 cm^{-1} a small peak is seen in the FT-VAC that is accentuated in the FT-DAC. In fact this is another area where experiment and theory disagree in Ref. 1. To further understand these differences, optimization and frequency calculations were conducted on protonated water clusters by including an argon atom in the system. The choice of argon is governed by the fact that argon is used in Ref. 1 and other similar studies[19,59] as a "messenger" where the weakly bound rare-gas atom is attached to the ion and then isolated for interaction with the laser using a mass spectrometer.[19,59] Photon absorption is monitored by mass loss upon argon evaporation. It is of interest to investigate if the IR spectrum changes in the presence of argon.

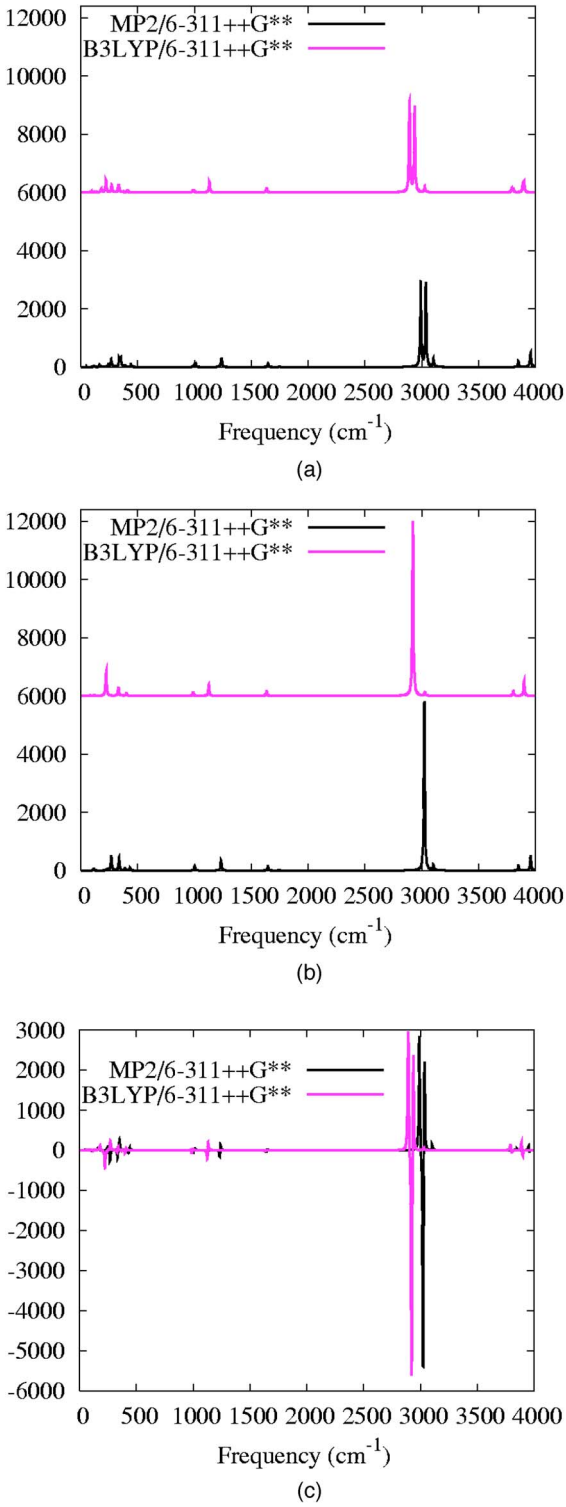

FIG. 8. (Color online) The spectral features for the (a) Eigen-argon complex, (b) Eigen complex, and (c) the difference spectrum which shows the effect of argon, using MP2 and B3LYP methodologies. In (a) and (b) the B3LYP spectrum is shown on the top and the MP2 spectrum is on the bottom. The frequency shifts between the two methodologies in the presence of argon, as seen in (a), are quite similar to those obtained in the absence of argon, seen in (b). The polarization of the argon and water, and the presence of the positive charge make the interaction between the argon and hydrogen partially electrostatic and is responsible for the acceptable agreement between the two methodologies. Note that in (c), the presence of argon produces a large change in intensity in the OH stretch for the protonated oxygen. This is also clear from the reduction in peak height seen in (a).

Downloaded 01 Sep 2005 to 129.79.138.80. Redistribution subject to AIP license or copyright, see http://jcp.aip.org/jcp/copyright.jsp

To understand where the argon atom would prefer to bind on the protonated water cluster, MP2 optimizations were performed followed by frequency calculations for a single argon atom bound to an Eigen cation. The Eigen cation was chosen since it contained all the complexities that a larger protonated water cluster would possess and in addition it provided three essentially diverse argon binding sites: the argon atom could bind to any of the free hydrogens, free oxygens, or the protonated oxygen. Consequently, three different optimizations were considered at the MP2/6-311 $++G^{**}$ level of theory to evaluate the preferential binding of argon. These calculations were performed in a stepwise manner; the input structures were optimized using Hartree-Fock and the resultant geometry was used for MP2 optimization. It was found that the argon atom preferred to remain weakly bound to one of hydrogen atoms dangling from the cluster. In fact, all three optimizations converged to one that had the argon atom bound to a dangling hydrogen. Binding to the oxygens was evidently not stable, even for the protonated oxygen, perhaps due to the lone pairs of oxygen and argon interacting with each other.

Since the argon does favor binding to the dangling OH hydrogen, the resulting frequencies and geometries obtained from the MP2 calculation for the Ar-Eigen complex, with argon bound to the dangling OH hydrogen, were compared with those obtained from a B3LYP/6-311++G^{**} calculation. This comparison is important since for larger protonated water clusters, MP2 optimization with large basis sets could become prohibitively expensive. Hence it is important to benchmark these results with DFT for smaller clusters. As a result B3LYP optimization was considered and it was found that the optimized geometry obtained from the B3LYP calculation had a rms deviation of 0.0095 Å with respect to the optimized geometry obtained from the MP2 calculation. This essentially implies that the two optimized geometries are identical. The binding energies, $E_{\text{Ar-Eigen}}-E_{\text{Ar}}-E_{\text{Eigen}}$, obtained from B3LYP was 0.5 kcal/mol lower than that obtained and from MP2. This is to be expected since B3LYP does not have the required van der Waals interactions. The harmonic frequencies obtained from the two methodologies are shown in Fig. 8. There exists a difference in harmonic frequencies obtained using the two methodologies; however, this difference is comparable to that obtained in the absence of argon, shown in Fig. 8(b). This level of agreement between the two methods is not counterintuitive since the argon binding to the hydrogens does have a partial electrostatic nature. The argon atom is polarized by the partial change on the hydrogen atom and this is further accentuated by the presence of the positive charge. It would of course be quite difficult for B3LYP to obtain a meaningful binding for the Ar–O complex. In fact, the latter binding process is underestimated by B3LYP on account of the van der Waals nature of this interaction. In Fig. 8(c) the difference spectrum (difference between the spectra in the presence and absence of argon) for both MP2 and B3LYP produces a significant change in the intensity of the OH stretch corresponding to the protonated oxygen. This is the same region (ca. 2900 cm^{-1}) where the small peak in the FT-VAC and the corresponding accentuated peak in the FT-DAC are seen. These results seem to indicate that the presence of argon could in fact diminish this intensity. Furthermore, both B3LYP and MP2 display a doublet corresponding to the OH stretch in the presence of argon, and a singlet in the absence of it. This is to be expected based on the asymmetry of the cluster in the presence of argon. It is, however, important to note the reduction in intensity. The effect of argon for larger protonated water clusters is currently under investigation.

IV. CONCLUSIONS

In this paper a detailed dynamical study of the $H^+(H_2O)_{21}$ "magic" water cluster has been presented using both *ab initio* and empirical molecular-dynamics techniques, at many different temperatures. Based on these simulations it was concluded that the protonated species in this cluster resides on the surface. A detailed analysis of the vibrational properties of this cluster was also carried out. The vibrational analysis was conducted in two different ways. In one approach the harmonic frequencies were analyzed for the "inherent" structures in the dynamics. In the other approach the vibrational properties were obtained from autocorrelation functions of *ab initio* dynamics data. The results thus obtained were found to be very different from each other in the important 2000–3000-cm^{-1} frequency region. The dynamical autocorrelation results seem to match previous experiments[1] while the frequencies of the inherent structures do not match experiment and deviate in a fashion similar to the 0-Kelvin theoretical results noted in Ref. 1. We thus conclude that dynamical and finite-temperature effects play a critical role in defining the spectral properties of this system.

ACKNOWLEDGMENTS

One of the authors (G.A.V.) acknowledges the support of this research by the National Science Foundation (Grant No. CHE-0317132), and another author (S.S.I.) acknowledges the Camille and Henry Dreyfus Foundation and the Chemistry department at Indiana University, Bloomington. We acknowledge Professor Krishnan Raghavachari for useful discussions on the subject.

[1] J.-W. Shin, N. I. Hammer, E. G. Diken *et al.*, Science **304**, 1137 (2004).
[2] M. Miyazaki, A. Fujii, T. Ebata, and N. Mikami, Science **304**, 1134 (2004).
[3] T. S. Zwier, Science **304**, 1119 (2004).
[4] C.-C. Wu, C.-K. Lin, H.-C. Chang, J.-C. Jiang, J.-L. Kuo, and M. L. Klein, J. Chem. Phys. **122**, 074315 (2005).
[5] N. Agmon, Chem. Phys. Lett. **244**, 456 (1995).
[6] R. P. Bell, *The Proton in Chemistry* (Cornell University Press, Ithaca, NY, 1973).
[7] M. Eigen and L. D. Maeyer, Proc. R. Soc. London, Ser. A **247**, 505 (1958).
[8] M. Eigen, Angew. Chem., Int. Ed. Engl. **3**, 1 (1964).
[9] G. Zundel, *The Hydrogen Bond-Recent Developments in Theory and Experiments* (North-Holland, Amsterdam, 1976), Chap. II, pp. 683–766.
[10] D. Eisenberg and W. Kauzman, *The Structure and Properties of Water* (Oxford University Press, Oxford, 1969).
[11] M. M. Teeter, Proc. Natl. Acad. Sci. U.S.A. **81**, 6014 (1984).
[12] S. Neidle, H. M. Berman, and H. S. Shieh, Nature (London) **288**, 129 (1980).
[13] L. A. Lipscomb, M. E. Peek, F. X. Zhou, J. A. Bertrand, D. VanDerveer, and L. D. Williams, Biochemistry **33**, 33 (1994).
[14] C. Tu, R. S. Rowlett, B. C. Tripp, J. G. Ferry, and D. N. Silverman, Biochemistry **41**, 15429 (2002).

Downloaded 01 Sep 2005 to 129.79.138.80. Redistribution subject to AIP license or copyright, see http://jcp.aip.org/jcp/copyright.jsp

[15] M. J. McEwan and L. F. Phillips, *Chemistry of the Atmosphere* (Eward Arnold, London, 1975).
[16] R. P. Wayne, *Chemistry of the Atmosphere* (Clarendon, Oxford, 1994).
[17] X.-D. Xiao, V. Vogel, and Y. R. Shen, Chem. Phys. Lett. **163**, 555 (1989).
[18] C. Radüge, V. Pflumio, and Y. R. Shen, Chem. Phys. Lett. **274**, 140 (1997).
[19] M. Okumura, L. I. Yeh, J. D. Myers, and Y. T. Lee, J. Phys. Chem. **94**, 3416 (1990).
[20] T. F. Magnera, D. E. David, and J. Michl, Chem. Phys. Lett. **182**, 363 (1991).
[21] X. Yang, X. Zhang, and A. W. Castleman, Jr., Int. J. Mass Spectrom. Ion Processes **109**, 339 (1991).
[22] S. Wei, Z. Shi, and A. W. Castleman, Jr., J. Chem. Phys. **94**, 3268 (1991).
[23] U. Achatz, B. S. Fox, M. K. Beyer, and V. E. Bondybey, J. Am. Chem. Soc. **123**, 6151 (2001).
[24] S.-W. Lee, H. Cox, W. A. Goddard, and J. L. Beauchamp, J. Am. Chem. Soc. **122**, 9201 (2000).
[25] M. Meot-Ner (Mautner), S. Scheiner, and W. O. Yu, J. Am. Chem. Soc. **120**, 6980 (1998).
[26] R. M. Lynden-Bell and J. C. Rasaiah, J. Chem. Phys. **105**, 9266 (1996).
[27] J. Lobaugh and G. A. Voth, J. Chem. Phys. **104**, 2056 (1996).
[28] R. Pomes and B. Roux, Biophys. J. **71**, 19 (1996).
[29] R. Pomes and B. Roux, J. Phys. Chem. **100**, 2519 (1996).
[30] H. Decornez, K. Drukker, and S. Hammes-Schiffer, J. Phys. Chem. A **103**, 2891 (1999).
[31] M. L. Brewer, U. W. Schmitt, and G. A. Voth, Biophys. J. **80**, 1691 (2001).
[32] C. J. Tsai and K. D. Jordan, Chem. Phys. Lett. **213**, 181 (1993).
[33] S. S. Xantheas, J. Chem. Phys. **100**, 7523 (1994).
[34] S. S. Xantheas, J. Chem. Phys. **102**, 4505 (1995).
[35] S. Sadhukhan, D. Munoz, C. Adamo, and G. E. Scuseria, Chem. Phys. Lett. **306**, 83 (1999).
[36] Y. Xie, R. B. Remington, and H. F. Schaefer III, J. Chem. Phys. **101**, 4878 (1994).
[37] L. Ojamae, I. Shavitt, and S. J. Singer, Int. J. Quantum Chem., Quantum Chem. Symp. **29**, 657 (1995).
[38] L. Ojamae, I. Shavitt, and S. J. Singer, J. Chem. Phys. **109**, 5547 (1998).
[39] S. J. Singer, S. McDonald, and L. Ojamae, J. Chem. Phys. **112**, 710 (2000).
[40] C. V. Cristian, L. Ojamae, I. Shavitt, and S. J. Singer, J. Chem. Phys. **113**, 5321 (2000).
[41] H.-P. Cheng, J. Phys. Chem. A **102**, 6201 (1998).
[42] R. R. Sadeghi and H.-P. Cheng, J. Chem. Phys. **111**, 2086 (1999).
[43] H.-P. Cheng and J. L. Krause, J. Chem. Phys. **107**, 8461 (1997).
[44] D. Wei and D. R. Salahub, J. Chem. Phys. **106**, 6086 (1997).
[45] E. S. Kryachko, Chem. Phys. Lett. **314**, 353 (1999).
[46] M. E. Tuckerman, K. Laasonen, M. Sprik, and M. Parrinello, J. Phys. Chem. **99**, 5749 (1995).
[47] D. Marx, M. E. Tuckerman, J. Hutter, and M. Parrinello, Nature (London) **397**, 601 (1999).
[48] A. Banerjee, R. Shepard, and J. Simons, J. Chem. Phys. **73**, 1814 (1980).
[49] A. Banerjee, A. Quigley, R. F. Frey, D. Johnson, and J. Simons, J. Acoust. Soc. Am. **109**, 1038 (1987).
[50] P. M. Holland and A. W. Castleman, Jr., J. Chem. Phys. **72**, 5984 (1980).
[51] H. B. Schlegel, J. M. Millam, S. S. Iyengar, G. A. Voth, A. D. Daniels, G. E. Scuseria, and M. J. Frisch, J. Chem. Phys. **114**, 9758 (2001).
[52] S. S. Iyengar, H. B. Schlegel, J. M. Millam, G. A. Voth, G. E. Scuseria, and M. J. Frisch, J. Chem. Phys. **115**, 10291 (2001).
[53] H. B. Schlegel, S. S. Iyengar, X. Li, J. M. Millam, G. A. Voth, G. E. Scuseria, and M. J. Frisch, J. Chem. Phys. **117**, 8694 (2002).
[54] S. S. Iyengar, H. B. Schlegel, G. A. Voth, J. M. Millam, G. E. Scuseria, and M. J. Frisch, Isr. J. Chem. **42**, 191 (2002).
[55] N. Rega, S. S. Iyengar, G. A. Voth, H. B. Schlegel, T. Vreven, and M. J. Frisch, J. Phys. Chem. B **108**, 4210 (2004).
[56] S. S. Iyengar and M. J. Frisch, J. Chem. Phys. **121**, 5061 (2004).
[57] T. J. F. Day, A. V. Soudachov, M. Cuma, U. W. Schmitt, and G. A. Voth, J. Chem. Phys. **117**, 5839 (2002).
[58] C. J. Burnham, M. K. Petersen, T. J. F. Day, S. S. Iyengar, and G. A. Voth (unpublished).
[59] E. G. Diken, J. M. Headrick, J. R. Roscioli, J. C. Bopp, M. A. Johnson, and A. B. McCoy, J. Phys. Chem. A **109**, 1487 (2005).
[60] M. J. Frisch, G. W. Trucks, H. B. Schlegel *et al.*, GAUSSIAN 03, revision b.02 Gaussian, Inc., Pittsburgh, PA, 2003.
[61] W. Smith and T. R. Forester, DL_POLY, a package of molecular simulation routines, The Council for the Central Laboratory of the Research Councils, Daresbury Laboratory at Daresbury, Nr. Warrington, 1999.
[62] U. W. Schmitt and G. A. Voth, J. Phys. Chem. B **102**, 5547 (1998).
[63] U. W. Schmitt and G. A. Voth, J. Chem. Phys. **111**, 9361 (1999).
[64] F. Wang and G. A. Voth, J. Chem. Phys. **122**, 144105 (2005).
[65] M. K. Petersen, S. S. Iyengar, T. J. F. Day, and G. A. Voth, J. Phys. Chem. B **108**, 14804 (2004).
[66] M. L. Brewer, U. W. Schmitt, and G. A. Voth, Biophys. J. **80**, 1691 (2001).
[67] A. M. Smondyrev and G. A. Voth, Biophys. J. **82**, 1460 (2001).
[68] A. M. Smondyrev and G. A. Voth, Biophys. J. **83**, 1987 (2002).
[69] Y. Wu and G. A. Voth, Biophys. J. **85**, 864 (2003).
[70] G. A. Voth, Front. Biosci. **8**, 1384 (2003).
[71] B. Ilan, E. Tajkhorshid, K. Schulten, and G. A. Voth, Proteins: Struct., Funct., Bioinf. **55**, 223 (2004).
[72] H. Lapid, N. Agmon, M. K. Petersen, and G. A. Voth, J. Chem. Phys. (in press).
[73] C. J. Burnham and S. S. Xantheas, J. Chem. Phys. **116**, 5115 (2002).
[74] U. H. E. Hansmann, Chem. Phys. Lett. **281**, 140 (1997).
[75] M. P. Hodges and D. J. Wales, Chem. Phys. Lett. **324**, 279 (2000).
[76] M. L. Connolly, Science **221**, 709 (1983).
[77] S. S. Iyengar, T. J. F. Day, and G. A. Voth, Int. J. Mass. Spectrom. **241**, 197 (2005).
[78] P. H. Berens, S. R. White, and K. R. Wilson, J. Chem. Phys. **75**, 515 (1981).
[79] J. S. Bader and B. J. Berne, J. Chem. Phys. **100**, 8359 (1994).
[80] J. Kim, U. W. Schmitt, J. A. Gruetzmacher, G. A. Voth, and N. F. Scherer, J. Chem. Phys. **116**, 737 (2002).
[81] C. P. Lawrence, A. Nakayama, N. Makri, and J. L. Skinner, J. Chem. Phys. **120**, 6621 (2004).
[82] F. J. Devlin and P. J. Stephens, J. Acoust. Soc. Am. **121**, 7413 (1999).
[83] E. L. Eliel, N. Allinger, S. J. Angyal, and G. A. Morrison, *Conformational Analysis* (Wiley-Interscience, New York, 1965).

Downloaded 01 Sep 2005 to 129.79.138.80. Redistribution subject to AIP license or copyright, see http://jcp.aip.org/jcp/copyright.jsp